Non-modal stability in Hagen-Poiseuille flow of a Bingham fluid

Rong Liu and Qiu Sheng Liu

Citation: Physics of Fluids (1994-present) **26**, 014102 (2014); doi: 10.1063/1.4861025
View online: http://dx.doi.org/10.1063/1.4861025
View Table of Contents: http://scitation.aip.org/content/aip/journal/pof2/26/1?ver=pdfcov
Published by the AIP Publishing

PHYSICS OF FLUIDS **26**, 014102 (2014)

Non-modal stability in Hagen-Poiseuille flow of a Bingham fluid

Rong Liu[a] and Qiu Sheng Liu[b]
Key Laboratory of Microgravity (National Microgravity Laboratory), Institute of Mechanics, Chinese Academy of Sciences, Beijing 100190, China

(Received 28 March 2013; accepted 21 November 2013; published online 7 January 2014)

Linear stability in Hagen-Poiseuille flow of a Bingham fluid is considered. Bingham fluid exhibits a yield stress in addition to a plastic viscosity. A Bingham number B, which describes the ratio of yield and viscous stresses, is used to characterize the behavior of Bingham-Hagen-Poiseuille flow. The effects of B on the stability are investigated using the energy method and the non-modal stability theory. The energy analysis shows that the non-axisymmetric disturbance has the lowest critical energy Reynolds number for all B. The global critical energy Reynolds number Re_g increases with B. At sufficient large B, Re_g has the order of $B^{1/2}$. For the non-modal stability, we focus on response to external excitations and initial conditions. The former is studied by examining the ϵ-pseudospectrum, and the latter is by examining the energy growth function $G(t)$. For the problem of response to external excitations, the maximum response is achieved by non-axisymmetric and streamwise uniform disturbances at the frequency of $\omega = 0$, with a possible choice of the azimuthal wavenumbers of $n = 1$, 2, or 3. For the problem of response to initial conditions, it is found that there can be a rather large transient growth even though the linear operator of the Bingham-Hagen-Poiseuille flow has no unstable eigenvalue. For small B, the optimal disturbance is in the form of streamwise uniform vortices and streaks. For large B, the optimal disturbance is in the form of oblique waves. The optimal energy growth decreases and the optimal azimuthal wavenumber increases with the increase of B. © *2014 AIP Publishing LLC*. [http://dx.doi.org/10.1063/1.4861025]

I. INTRODUCTION

Flows of viscoplastic fluids occur in many industrial processes, for example, in oil wells, especially during drilling and cementing operations, and also in the food processing and in mining industries.[1] The fluid behavior of a viscoplastic material is characterized by the existence of a yield stress (τ_0) below which the material exhibits solid-like behavior and beyond which it exhibits liquid-like behavior. Most natural and industrial materials (glues, inks, pastes, slurries, paints, emulsions, foodstuffs, blood, drilling muds, etc.) obtained by suspending a large number of particles interacting via colloidal forces or direct contact in water fall into this category exhibiting a yield stress.[2] This yield stress is in fact the strength necessary to break the continuous network of interactions between particles throughout the sample.

The Bingham model is widely used to describe the rheological behavior of a viscoplastic fluid. The constitutive laws are formulated by as

$$\boldsymbol{\tau} = \left(\frac{\tau_0}{\dot{\gamma}} + \mu_0\right)\dot{\boldsymbol{\gamma}} \Leftrightarrow \tau \geq \tau_0,$$
$$\dot{\gamma} = 0 \Leftrightarrow \tau < \tau_0, \tag{1}$$

[a]Electronic mail: liurong@imech.ac.cn
[b]Electronic mail: liu@imech.ac.cn

where $\dot{\boldsymbol{\gamma}}$ is the rate of strain, $\boldsymbol{\tau}$ is the stress tensor, $\dot{\gamma}$ and τ are the second invariants of the rate-of-strain and deviatoric stress tensors, respectively. We note that from the experimental point of view, more complex models such as the Herschel-Bulkley model can be more accurate to describe the viscoplastic behavior. However, the most important features of viscoplastic fluid flows, i.e., a yield stress and a shear-thinning behavior of the effective viscosity are contained by the simple Bingham model.

The transition from laminar to turbulent flow in a circular pipe or in a plane channel is one of the most intriguing problems of classical hydrodynamics since the original work of Reynolds.[3] However, an understanding of the mechanism of transition from laminar towards turbulence is far from complete, even for Newtonian fluids.

Traditionally, a first step in investigating transition is the normal-mode analysis. For this approach, it is assumed that each mode has an exponential time dependence, thus the base flow is considered to be unstable if an eigenvalue is found in the unstable complex half plane. It is well known that the pipe Poiseuille flow (Hagen-Poiseuille flow) is linear stable at all Reynolds numbers[4,5] (here, $Re = UD/\nu$ where U is the mean speed, D is the diameter of the pipe, and ν is the kinematic viscosity of the fluid). However, in most experiments of pipe Poiseuille it is found that the transitional Reynolds number depends on the level of disturbance in the flow. Transition in a circular pipe flow is observed at $Re \approx 2000$, whereas, in carefully designed experiments the transition point can be delayed to Reynolds numbers as large as $Re \approx 100\,000$.[6] Peixinho and Mullin[7] have performed a novel experiment to provide direct evidence for critical point behavior in the problem of the transition to turbulence in a pipe. Their experimental facility enabled a laminar flow to be achieved up to a flow rate corresponding to $Re = 23\,000$. For more experimental and theoretical works on the transition to turbulence in pipe flow, we refer the reader to the review articles[8,9] and references therein. Similar discrepancies between the computed critical Reynolds number of linear stability analysis and the observed transitional Reynolds number in experiments also exist in other simple flows, such as Couette and Poiseuille flows.[10,11]

Until now, no full theory of transition to turbulence in shear flows exists. Nevertheless, significant progress has been achieved due to the emergence of the non-modal stability theory. In the normal-mode analysis, a common simplification is the assumption that each mode has an exponential time dependence. The behavior of each mode is inferred from the spectrum of the governing linear operator. The base flow is considered to be unstable if an eigenvalue is found in the unstable complex half-plane. For most wall-bounded shear flows, because of the non-normality of the governing linear operator, the spectrum is a poor proxy for the disturbance behavior as it only describes the long-term behavior of the perturbation. The main point of departure of the non-modal theory from the traditional eigenvalue analysis is the fact that even if all of the eigenvalues of a linear system are distinct and lie well inside the stable half-plane, inputs to that system may be amplified by substantially large factors if the linear operator is non-normal.[12] Trefethen *et al.*[10] addressed the general concept of the non-modal stability theory and studied the transient behavior for plane Poiseuille flow and plane Couette flow. Plane Poiseuille flow, plane Couette flow, and pipe Poiseuille flow have been extensively studied in the framework of the non-modal theory.[4,11,13] A common conclusion of the these studies is that disturbance may experience a substantial amplification even for exponentially damped modes because of the transient growth mechanism. The optimal disturbance is in the form or close to the form of streaks. The so called "lift-up" effect is responsible for the amplification of the optimal disturbance from streamwise vortices to alternating low and high velocity streaks in the streamwise velocity component.[14–16] This mechanism works by efficiently extracting momentum from the mean flow and transferring it to the perturbation. Mathematically speaking, the non-modal theory offers an explanation of why these streamwise streaks are so common: even though these structures are not eigenmodes of the linearized flow problem, they are pseudomodes.[10]

We should note that the results of non-modal theory are basically linear. Given the apparently potent linear amplification of the optimal disturbances predicted by non-modal theory, interest was naturally focused on how energy of the disturbance can be sustained after a substantial transient growth. It is naturally believed that a sufficient growth of the optimal disturbances may trigger strongly nonlinear mechanisms capable of sustaining turbulence. However, the kinetic energy of

optimal disturbance predicted by the non-modal approach will eventually decay and the optimal disturbance in the form of streamwise uniform vortices and streaks is not able to trigger transition.[17] Waleffe[18] proposed the "Self-Sustaining Process" (SSP) to understand how turbulence is maintained at low Reynolds numbers. The SSP consists of three distinct phases: formation of streamwise streaky flow by streamwise vortices, instability of streaky flow, and the regeneration of the streamwise vortices. During streak breakdown, a set of nonlinear interactions re-energizes the streamwise vortices, leading to formation of a new set of streaks, and completing the regeneration cycle. In the SSP cycle, the mechanism of the transient growth is responsible for the formation of streaks. Even though the non-modal analysis is basically linear, it may provide a lower bound of the Reynolds number for the transition and predicts possible initial conditions most likely to be responsible for the transition.

For many industrial applications, the control of flows of a yield-stress fluid requires knowledge of determining the flow regime and in particular of the conditions for stability and transition to turbulence. Consequently, as with Newtonian flows, studies of stability and transition for flows of yield-stress fluids have remained a problem of practical interest over the years. Frigaard *et al.*[19] studied the linear stability with respect to two-dimensional disturbances of plane Poiseuille flow of a Bingham fluid using a modal approach. However, the results are incomplete because even symmetry for the eigenfunction of the vertical velocity was imposed. Nouar and Frigaard[20] performed a nonlinear stability analysis based on the energy method. The results showed that the critical energy Reynolds number, Re, increases with Bingham number, B, at least as fast as $Re \sim B^{1/2}$ as $B \to \infty$. In general, for non-Newtonian fluids Squire's theorem is not valid. In these cases, three-dimensional disturbance must be considered for stability problems. Frigaard and Nouar[21] investigated the problem of eigenvalue bounds for three-dimensional disturbances in plane Bingham-Poiseuille flow (PBPF). The authors showed that three-dimensional linear stability can be achieved for a Reynolds number bound of form $Re = O(B^{3/4})$ as $B \to \infty$. Recently, Nouar *et al.*[22] investigated the stability of plane Bingham-Poiseuille flow in the framework of the non-modal theory. The results showed that the optimal disturbance consists of almost streamwise vortices as $B \ll 1$, whereas the optimal disturbance becomes oblique for large B.

The works on the stability of Bingham fluid mentioned above focus on plane channel flows. Escudier and Presti[23] and Escudier *et al.*[24] studied experimentally the flow structure of a yield stress fluid in a cylindrical pipe. The result showed that asymmetrical flow behavior exists in transitional pipe flow. Peixinho *et al.*[25] presented an experimental study on laminar transitional and turbulent flow in a pipe of a yield stress fluid, a shear thinning fluid without yield stress and a Newtonian fluid. The results showed that the transition for the yield stress fluid takes place in two stages. First, low frequency oscillations of the axial velocity are observed in the annular zone. The experimental velocity profile departs slightly from the laminar theoretical solution. Then, with increasing the Reynolds number, turbulent spots appear to fill up the whole section. Esmael and Nouar[26] showed that a robust nonlinear coherent structure characterized by two weakly modulated counter-rotating longitudinal vortices exists in transitional flow. Esmael[27] performed in his Ph.D. thesis a three-dimensional linear stability analysis for a pipe flow of a yield-stress fluid described by the Herschel-Bulkley model. It is found that the nonlinear coherent structure in Ref. 26 is similar to the suboptimal disturbance in the form streamwise uniform streaks with the azimuthal wavenumber $m = 1$ instead of the optimal disturbance with $m = 2$. Further experiments were performed by Esmael *et al.*[26] to show that this nonlinear asymmetric state is a weakly turbulent flow induced by shear-thinning behavior. Recently, Güzel *et al.*[28] investigated experimentally the transition to turbulence of Hagen-Poiseuille flow of a yield stress fluid. Their results indicated that transition occurs only when the Reynolds stresses of the flow equal or exceed the yield stress of the fluid, i.e., the plug is broken before transition commences. Most of the works mentioned above focus on experimental work on laminar and transitional flow in yield stress flow in a pipe. However, a careful look at previous works indicates that the theoretical works on the stability of pipe Poiseuille flow of a Bingham fluid are very limited. Sine a pipe Poiseuille flow has been believed to be linearly stable, it seems that study of the modal linear stability of Bingham fluid flow is non-productive. In the present paper, we will study the non-modal stability of Bingham-Hagen-Poiseuille flow (BHPF). The purpose of the present paper is to understand the effect of the behavior of viscoplasticity on the

non-modal stability, including response to excitations and optimal disturbances in the form of initial conditions in Bingham-Hagen-Poiseuille flow.

The paper is organized as follows. In Sec. II, the mathematical formulation of the physical model is presented. In Sec. III, the numerical method is presented. In Sec. IV, we present the results and discussions. In Sec. V, we summarize the results and present the conclusions.

II. MATHEMATICAL FORMULATION

A. Physical model

A pipe flow of an incompressible Bingham fluid with a yield stress τ_0 and a plastic viscosity μ_0 is considered. The flow is driven by a constant pressure gradient along the axis of the pipe. As shown in Fig. 1, R is the radius of the pipe, r_0 is the radius of the unyielded zone, $d = R - r_0$ is the width of the yielded zone, and U_0 is the maximum velocity of the base flow. To assess the effect of yield stress on the instability of pipe flows, it is important to employ an appropriate length scale. Because the flow is confined in the yielded zone, it is appropriate to use d as the length scale instead of R. In the controlling equations, we choose the scales of length, time, velocity, and pressure as d, d/U_0, U_0, and ρU_0^2. The Navier-Stokes equations are expressed in dimensionless form as

$$\nabla \cdot \boldsymbol{u} = 0, \tag{2}$$

$$\frac{\partial \boldsymbol{u}}{\partial t} + \boldsymbol{u} \cdot \nabla \boldsymbol{u} = -\nabla p + \nabla \cdot \boldsymbol{\tau}, \tag{3}$$

where p is the pressure, $\boldsymbol{\tau}$ is the stress tensor, and $\boldsymbol{u} = u\mathbf{e}_r + v\mathbf{e}_\theta + w\mathbf{e}_z$ is the velocity vector, in which u, v, w are the velocity components and $\mathbf{e}_r$, $\mathbf{e}_\theta$, $\mathbf{e}_z$ are the unit vectors in the radial, the azimuthal, and the axial directions.

The constitutive equations for Bingham fluids are

$$\boldsymbol{\tau} = \frac{1}{Re}\mu\dot{\boldsymbol{\gamma}} \Leftrightarrow \tau > \frac{B}{Re},$$

$$\dot{\gamma} = 0 \Leftrightarrow \tau \le \frac{B}{Re}, \tag{4}$$

where the effective viscosity is

$$\mu = 1 + \frac{B}{\dot{\gamma}}, \tag{5}$$

and $\dot{\gamma}$, τ are given by

$$\dot{\gamma} = [\frac{1}{2}\dot{\gamma}_{ij}\dot{\gamma}_{ij}]^{1/2}, \tau = [\frac{1}{2}\tau_{ij}\tau_{ij}]^{1/2}. \tag{6}$$

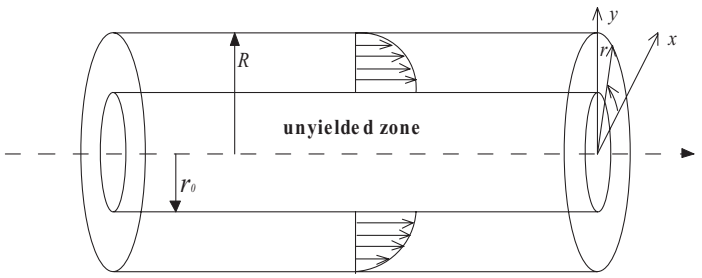

FIG. 1. Sketch of the geometry of a Bingham-Hagen-Poiseuille flow. (x, y, z) is a Cartesian coordinate system with z the axial coordinate along the cylinder. A cylindrical coordinate system (r, θ) is chosen at the cylinder centerline $r = 0$.

The two dimensionless parameters B and Re are, respectively, the Bingham number and the Reynolds number defined as

$$B = \frac{\tau_0 d}{\mu_0 U_0}, \quad Re = \frac{\rho U_0 d}{\mu_0}. \tag{7}$$

The basic flow considered is a steady one driven by an imposed pressure gradient $-P_0$ in the z-direction, i.e.,

$$p = -P_0 z. \tag{8}$$

The velocity of the base flow is one-dimensional and can be written in the form of $\bar{\boldsymbol{u}} = (0, 0, W(r))$. The expression of the axial velocity profile $W(r)$ is

$$W(r) = \begin{cases} 1, & 0 \le r < r^*, \\ \frac{B}{2r^*}[1 - (r - r^*)^2], & r^* \le r \le 1 + r^*, \end{cases} \tag{9}$$

where $r^* = r_0/d$ denotes the position of the yield surface. Since the maximum value of velocity has been used to scale the flow, it follows that

$$B = 2r^*. \tag{10}$$

As $B \to 0$, the unyielded zones is reduced to the centerline, and the velocity of the base state approaches the Newtonian case. With the increase of B the unyielded zone widens towards the wall. As $B \to \infty$, the unyielded zone fills almost the whole pipe.

In experiments, it is usual to use the radius R as the length scale. The Bingham number and the Reynolds number are defined as

$$\tilde{B} = \frac{\tau_0 R}{\mu_0 U_0}, \quad \tilde{Re} = \frac{\rho U_0 R}{\mu_0}. \tag{11}$$

The relations between B and $\tilde{B}$, and Re and $\tilde{Re}$ are

$$\frac{\tilde{B}}{B} = \frac{\tilde{Re}}{Re} = 1 + \frac{B}{2}. \tag{12}$$

As $B \to 0$, $\tilde{B} \sim B$. As $B \to \infty$, $\tilde{B} \sim B^2/2$.

B. Linear stability analysis

Following the classic linear stability analysis, our starting point for the analysis of infinitesimal disturbances $(\boldsymbol{u}', p')$ is to linearize the Navier-Stokes equation around the primary flow $(\bar{\boldsymbol{u}}, \bar{p})$. The linearized perturbation equations in the yielded zones are as follows:

$$\nabla \cdot \boldsymbol{u}' = 0, \tag{13}$$

$$\frac{\partial \boldsymbol{u}'}{\partial t} + \boldsymbol{u}' \cdot \nabla \bar{\boldsymbol{u}} + \bar{\boldsymbol{u}} \cdot \nabla \boldsymbol{u}' = -\nabla p' + \nabla \cdot \boldsymbol{\tau}', \tag{14}$$

where

$$\boldsymbol{\tau}' = \frac{1}{Re}(\mu' \bar{\dot{\boldsymbol{\gamma}}} + \bar{\mu} \dot{\boldsymbol{\gamma}}'), \tag{15}$$

in which

$$\bar{\mu} \dot{\boldsymbol{\gamma}}' = \dot{\boldsymbol{\gamma}}' + \frac{B}{\dot{\gamma}(\bar{\boldsymbol{u}})} \dot{\boldsymbol{\gamma}}'. \tag{16}$$

The viscosity perturbation μ' can be expressed as

$$\mu' = \frac{\mathrm{d}\mu}{\mathrm{d}\dot{\gamma}} \mid_{\boldsymbol{u}=\bar{\boldsymbol{u}}} \dot{\gamma}' = \frac{\mathrm{d}\mu}{\mathrm{d}\dot{\gamma}} \mid_{\boldsymbol{u}=\bar{\boldsymbol{u}}} \mathrm{Sgn}(\bar{\dot{\gamma}}_{zr}) \dot{\gamma}'_{zr}. \tag{17}$$

It can be shown straightforwardly that

$$\tau'_{ij} = \bar{\mu}\dot{\gamma}'_{i,j} \quad for \quad ij \neq rz, zr,$$
$$\tau'_{ij} = \mu_t\dot{\gamma}'_{i,j} \quad for \quad ij = rz, zr, \tag{18}$$

in which μ_t is the tangent viscosity defined as $\mu_t = \bar{\mu} + \frac{\mathrm{d}\mu}{\mathrm{d}\dot{\gamma}}\,|_{\boldsymbol{u}=\bar{\boldsymbol{u}}}\,\bar{\dot{\gamma}}$. For a non-Newtonian fluid, the difference between μ_t and $\bar{\mu}$ identifies the departure from Newtonian viscosity. For a Bingham fluid, it can be shown that

$$\mu_t - \bar{\mu} = -\frac{B}{\dot{\gamma}(\bar{\boldsymbol{u}})}. \tag{19}$$

At last we obtain the divergence of perturbed stress tensor as

$$\boldsymbol{\nabla}\cdot\boldsymbol{\tau}' = \frac{1}{Re}\{\bar{\mu}\nabla^2\boldsymbol{u}' + \frac{\mathrm{d}\bar{\mu}}{\mathrm{d}r}\mathbf{e}_r\cdot\dot{\boldsymbol{\gamma}}' + (\mu_t - \bar{\mu})\frac{\partial\dot{\gamma}'_{zr}}{\partial z}\mathbf{e}_r + \frac{1}{r}\frac{\partial r(\mu_t - \bar{\mu})\dot{\gamma}'_{rz}}{\partial r}\mathbf{e}_z\}. \tag{20}$$

For $B > 0$, it is assumed that the position of the yield surface undergoes an initially infinitesimal perturbation, during which the unyielded zone persists, and then the perturbation develops from its initial position. Some justification for this assumption can be found in Ref. 19. The yielded surface can be linearly perturbed from its initial position,

$$r_Y = r^* + h, \tag{21}$$

in which r_Y denotes the yield surface position, h denotes the disturbance of the surface with respect to the initial position. As the flow is periodic in the azimuthal direction and is assumed periodic in the streamwise direction, all solutions to the linearized controlling equations can be expressed as superpositions of complex Fourier modes of the form

$$[\boldsymbol{u}'(r,\theta,z,t),\, p'(r,\theta,z,t),\, h(z,t)] = [\hat{\boldsymbol{u}}(r,t),\, \hat{p}(r,t),\, h(t)]e^{i(n\theta+kz)}, \tag{22}$$

in which the streamwise wavenumber $k \in \mathscr{R}$, and the azimuthal wavenumber $n \in \mathscr{Z}$.

At last the flowing initial value problem is obtained:

$$\mathtt{D}\hat{u} + \frac{\hat{u}}{r} + \frac{in}{r}\hat{v} + ik\hat{w} = 0, \tag{23}$$

$$\frac{\partial\hat{u}}{\partial t} = -\mathtt{D}\hat{p} - ikW\hat{u} + \frac{\bar{\mu}}{Re}[(\mathtt{D}^2 + \frac{\mathtt{D}}{r})\hat{u} - (\frac{n^2+1}{r^2} + k^2)\hat{u} - \frac{2in}{r^2}\hat{v}] + \frac{1}{Re}[2\mathtt{D}\bar{\mu}\mathtt{D}\hat{u} + (\mu_t - \bar{\mu})(ik\mathtt{D}\hat{w} - k^2\hat{u})], \tag{24}$$

$$\frac{\partial\hat{v}}{\partial t} = -\frac{in}{r}\hat{p} - ikW\hat{v} + \frac{\bar{\mu}}{Re}[(\mathtt{D}^2 + \frac{\mathtt{D}}{r})\hat{v} - (\frac{n^2+1}{r^2} + k^2)\hat{v} + \frac{2in}{r^2}\hat{u}] + \frac{\mathtt{D}\bar{\mu}}{Re}[\frac{in}{r}\hat{u} + \mathtt{D}\hat{v} - \frac{\hat{v}}{r}], \tag{25}$$

$$\frac{\partial\hat{w}}{\partial t} = -ik\hat{p} - ikW\hat{w} - \hat{u}\mathtt{D}W + \frac{1}{Re}[(\mathtt{D}^2 + \frac{\mathtt{D}}{r})\hat{w} - (\frac{n^2}{r^2} + k^2)\hat{w}] + \frac{1}{Re}\frac{B}{\dot{\gamma}(\bar{\boldsymbol{u}})}[-(\frac{n^2}{r^2} + k^2)\hat{w} - ik(\mathtt{D} + \frac{1}{r})\hat{u}], \tag{26}$$

in which $\mathtt{D} \equiv \partial/\partial r$.

The boundary conditions at the pipe wall ($r = 1 + r^*$) are given by the no-slip assumption

$$\hat{u} = \hat{v} = \hat{w} = 0. \tag{27}$$

Assuming $k \neq 0$ or $n \neq 0$, the boundary conditions at the unperturbed yield surface, $r = r^*$, are

$$\hat{u} = \hat{v} = \hat{w} = 0, \tag{28}$$

$$\mathrm{D}\hat{u} = \mathrm{D}\hat{v} = 0, \mathrm{D}\hat{w} = -h\mathrm{D}^2 W. \tag{29}$$

The boundary conditions for a plane Bingham-Poiseuille flow has been derived by Nouar *et al.*[19] For a pipe Poiseuille flow of a Bingham fluid, derivation of the boundary conditions is similar to that of the plane Poiseuille flow. The Dirichlet boundary conditions $\boldsymbol{u}' = 0$ at the yield surface come from the fact that the unyielded plug zone is constrained to move as a rigid body according to the Bingham model. With the help of velocity continuity across the yield surface, it follows that the fluid particles at the yield surface satisfy

$$\frac{\partial}{\partial\theta}\boldsymbol{u}' = \frac{\partial}{\partial z}\boldsymbol{u}' = 0. \tag{30}$$

The Neumann conditions come from linearization of the condition $\dot{\boldsymbol{\gamma}}(\bar{\boldsymbol{u}} + \boldsymbol{u}') = 0$, at the perturbed yield surface, onto the unperturbed yield surface position.

Note that the equations and boundary conditions are valid for $k \neq 0$ or $n \neq 0$. For the case of $k = 0$ and $n = 0$, it is easy to find that $\hat{u} = 0$, $\hat{v} = 0$, and $\hat{p} = 0$. Thus, the stability problem reduces to a one-dimensional problem for $\hat{w}$ and h as

$$\frac{\partial\hat{w}}{\partial t} = \frac{1}{Re}(\mathrm{D}^2 + \frac{\mathrm{D}}{r})\hat{w}, \tag{31}$$

at the pipe wall $r = 1 + r^*$,

$$\hat{w} = 0, \tag{32}$$

at the yield surface $r = r^*$,

$$\mathrm{D}\hat{w} = -h\mathrm{D}^2 W, r^*\frac{\partial\hat{w}}{\partial t} = 2(\frac{d}{R})(\frac{\tau_w}{\tau_0})\frac{B}{Re}h. \tag{33}$$

Now we will show that there is no positive eigenvalue for the one-dimensional problem. Using the normal mode expansions, the disturbance can be written in the form of $(\hat{w}, h) \sim (\hat{w}(r), h)e^{\lambda t}$. Note that λ is real, since $\hat{w}$ is real. We assume that λ is a positive number. Non-trivial solution for $\hat{w}$ are $\hat{w} = A[I_0(\sqrt{Re\lambda}r)K_0(\sqrt{Re\lambda}(1 + r^*)) - I_0(\sqrt{Re\lambda}(1 + r^*))K_0(\sqrt{Re\lambda}r)]$. At last, we can obtain the dispersion relation

$$\begin{aligned}&\sqrt{Re\lambda}[I_0'(\sqrt{Re\lambda}r^*)K_0(\sqrt{Re\lambda}(1 + r^*)) - I_0(\sqrt{Re\lambda}(1 + r^*))K_0'(\sqrt{Re\lambda}r^*)]\\ &+\frac{\mathrm{D}^2 W(r^*)}{2}\frac{r^*\lambda R}{d}\frac{\tau_0}{\tau_w}\frac{Re}{B}[I_0(\sqrt{Re\lambda}r^*)K_0(\sqrt{Re\lambda}(1 + r^*)) - I_0(\sqrt{Re\lambda}(1 + r^*))K_0(\sqrt{Re\lambda}r^*)] = 0,\end{aligned} \tag{34}$$

in which I_0 and K_0 are the two linearly independent solutions to the 0 order modified Bessel's equation. Note that $\mathrm{D}^2 W(r^*) < 0$, $K_0'(x) < 0$, and $I_0'(x) < 0$ for all $x > 0$. Thus, $[I_0'(\sqrt{Re\lambda}r^*)K_0(\sqrt{Re\lambda}(1 + r^*)) - I_0(\sqrt{Re\lambda}(1 + r^*))K_0'(\sqrt{Re\lambda}r^*)] > 0$, and $[I_0(\sqrt{Re\lambda}r^*)K_0(\sqrt{Re\lambda}(1 + r^*)) - I_0(\sqrt{Re\lambda}(1 + r^*))K_0(\sqrt{Re\lambda}r^*)] < 0$. So, the left side of the dispersion relation is a positive number. This means there is no positive eigenvalue for the problem of $k = 0$ and $n = 0$.

For the non-modal stability, the two-dimensional Reynolds stress mechanism and the lift-up mechanism are responsible for the energy growth. These two mechanisms are absent in the case of $k = 0$ and $n = 0$. So, for the non-modal stability problem, we do not consider the case of $k = 0$ and $n = 0$.

III. NUMERICAL METHOD

The controlling equations (23)–(26) and the boundary conditions (27)–(29) can be expressed in vector form

$$\mathscr{B}\frac{\partial}{\partial t}\boldsymbol{q} = \mathscr{A}\boldsymbol{q}, \tag{35}$$

in which $\boldsymbol{q} = (\hat{u}, \hat{v}, \hat{w}, \hat{p}, h)^T$. Finally, we obtain the linear initial value problem

$$\frac{\partial}{\partial t}\boldsymbol{q} = -i\mathscr{L}\boldsymbol{q}, \tag{36}$$

in which $\mathscr{L} = i\mathscr{B}^{-1}\mathscr{A}$.

In the present paper, we will examine the non-modal stability, including the response to external excitations and initial conditions. Now we begin with the responses to external excitations. Suppose a fluid system is driven by a signal of the form

$$\boldsymbol{q}_{in}(x, y, z, t) = \exp(-i\omega t)\boldsymbol{Q}_{in}(x, y, z), \tag{37}$$

in which ω is the complex frequency. Then the response $\boldsymbol{q}_{out}(x, y, z, t)$ and the input signal $\boldsymbol{q}_{in}(x, y, z, t)$ satisfy the equation

$$\frac{\partial}{\partial t}\boldsymbol{q}_{out} = -i\mathscr{L}\boldsymbol{q}_{out} + \exp(-i\omega t)\boldsymbol{Q}_{in}. \tag{38}$$

From Eq. (38), we obtain the response $\boldsymbol{q}_{out}$ in the form of

$$\boldsymbol{q}_{out}(x, y, z, t) = i(\omega\mathscr{I} - \mathscr{L})^{-1}\boldsymbol{q}_{in}(x, y, z). \tag{39}$$

Here, $\mathscr{I}$ is the identity operator. The solution operator $(\omega\mathscr{I} - \mathscr{L})^{-1}$ is known as the resolvent. We denote the maximum amplification of a disturbance at frequency ω by $\mathcal{R}(\omega)$. $\mathcal{R}(\omega)$ is equal to the norm of the resolvent and expressed as

$$\mathcal{R}(\omega) = \max_{\boldsymbol{q}_{in}\neq 0} \frac{\| \boldsymbol{q}_{out} \|}{\| \boldsymbol{q}_{in} \|} = \| (\omega\mathscr{I} - \mathscr{L})^{-1} \| . \tag{40}$$

Here, $\| \cdot \|$ denotes a norm on $\mathbb{C}^N$, "max" denotes the maximum. An eigenvalue of $\mathscr{L}$ is a number ω such that $\| (\omega\mathscr{I} - \mathscr{L})^{-1} \| \to \infty$. Generalizing this result leads naturally to the definition of "ϵ − *pseudospectrum*."[29] For any $\epsilon \geq 0$, the "ϵ-pseudospectrum" of $\mathscr{L}$ is defined as

$$\Lambda_\epsilon(\mathscr{L}) = \{\omega \in \mathbb{C} : \|(\omega\mathscr{I} - \mathscr{L})^{-1}\| \geq \epsilon^{-1}\}. \tag{41}$$

Quest for maximum amplification of initial conditions is of particular interest in many hydrodynamic stability problems. For the linear system (36), the solution has the form

$$\boldsymbol{q}(t) = \exp(-i\mathscr{L}t)\boldsymbol{q}(0). \tag{42}$$

The maximum amplification of initial condition can be described by the growth function $G(t)$ as

$$G(t) = \max_{\boldsymbol{q}(0)\neq 0} \frac{\| \boldsymbol{q}(t) \|^2}{\| \boldsymbol{q}(0) \|^2} = \| e^{-i\mathscr{L}t} \|^2 . \tag{43}$$

We should note that $\mathcal{R}(\omega)$ and $G(t)$ are related to the choice of definition of the norm $\| \cdot \|$. In the present paper, we choose the norm $\| \cdot \|$ as the energy norm. For variable $\boldsymbol{q}$, we will make use of a scalar product based on energy density defined as

$$(\boldsymbol{q}_1, \boldsymbol{q}_2)_{\mathscr{M}} = \pi \int_{r^*}^{1+r^*} r[\hat{u}_1\hat{u}_2^* + \hat{v}_1\hat{v}_2^* + \hat{w}_1\hat{w}_2^*]\mathrm{d}r, \tag{44}$$

in which * denotes the complex conjugate. Based on this scalar product, the associated energy norm is given as follows:

$$\|\boldsymbol{q}\|_{\mathscr{M}}^2 = (\boldsymbol{q}, \boldsymbol{q})_{\mathscr{M}} = \pi \int_{r^*}^{1+r^*} r[|\hat{u}|^2 + |\hat{v}|^2 + |\hat{w}|^2]\mathrm{d}r. \tag{45}$$

For initial value problems in hydrodynamics, we may be interested in the energy growth rate at the initial stage. The concept of numerical range can be used to link the operator to the initial energy growth. The numerical range is defined as

$$W(\mathbf{A}) = \{\mathbf{x}^*\mathbf{A}\mathbf{x} : \mathbf{x} \in \mathbb{C}^N, \|\mathbf{x}\| = 1\}, \tag{46}$$

in which $\mathbf{A} \in \mathbb{C}^{N\times N}$. The numerical abscissa of $\mathbf{A}$ is defined as

$$\omega(\mathbf{A}) = \sup_{z\in W(\mathbf{A})} \mathrm{Re}(z) = \lim_{t\to 0} \frac{\mathrm{d}}{\mathrm{d}t}\|e^{\mathbf{A}t}\|. \tag{47}$$

The main application of numerical range is to the analysis of energy growth for initial value problems. The numerical abscissa of $-i\mathscr{L}$ corresponds to the initial growth rate of the energy growth function.[11,29]

The spectral method can yield great accuracy for hydrodynamic stability problems. In the present paper, a Chebyshev-collocation method is used to solve the eigenvalue problem. We first transform the domains of $[r^*, 1 + r^*]$ to the Chebyshev domain $[-1, 1]$ by introducing

$$\zeta = 2(r - r^*) - 1. \tag{48}$$

The variables $\hat{\boldsymbol{u}}$ and $\hat{p}$ are expanded as

$$\hat{\boldsymbol{u}} = \sum_{n=0}^{N} \hat{\boldsymbol{u}}_n T_n(\zeta),\ \hat{p} = \sum_{n=0}^{N} \hat{p}_n T_n(\zeta), \tag{49}$$

in which T_n denotes the nth Chebyshev polynomial.

Using the Chebyshev series (49) and substituting $\partial/\partial t$ with $-i\omega$, the governing equations can be written in discrete form

$$\mathcal{A}\mathbf{x} = \omega\mathcal{B}\mathbf{x}, \tag{50}$$

in which $\mathbf{x}$ is the vector consisting of the spectral coefficients of $\hat{\boldsymbol{u}}$ and $\hat{p}$, and $\mathcal{A}, \mathcal{B}$ arise from discretization of the controlling equations and boundary conditions. This system of equations is required to solve for $4N + 5$ unknowns. The numerical method for general eigenvalue problem in the form $\mathcal{A}\mathbf{x} = \omega\mathcal{B}\mathbf{x}$ has been described by Canuto *et al.* [30]

The computation of response to external forcing $\mathcal{R}(\omega)$ and the energy growth function $G(t)$ can be accomplished using an eigenvector expansion method in which eigenvectors are obtained from the Chebyshev-collocation method. For the procedure of this approach, we refer the reader to Refs. 4, 11.

IV. RESULTS AND DISCUSSIONS

For the stability problem of Bingham-Hagen-Poiseuille flow, the stability is determined by two parameters, i.e., the Reynolds number Re and the Bingham number B. For the energy stability problem, we will fix B and study the critical conditions of the Reynolds number. For non-modal stability problem, we will study the amplification of optimal disturbance. For most of Newtonian channel flows, the optimal disturbances are in the form of or close to streamwise independent vortices and streaks. For streamwise independent disturbance ($k = 0$), the optimal energy growth has the form of $G(t) = Re^2 f(t/Re)$ for Newtonian channel and pipe flows.[11,17] For Bingham-Hagen-Poiseuille flow, if the scaled time t/Re and velocity $\hat{\boldsymbol{u}}/Re$ are introduced, it can be easily shown that the optimal energy growth has the form $G(t) = Re^2 f(t/Re, B)$ for a given azimuthal wavenumber n at $k = 0$. For a given azimuthal wavenumber, results obtained for a particular Reynolds number can be scaled to a different Reynolds number in a straightforward manner. Thus, when investigating the optimal energy growth of the streamwise independent disturbance for the non-modal stability problem, we can fix Re and examine the influence of B on the problem. In most of the results, we fixed the Reynolds number at $Re = 3000$. It is convenient to convert the results of $Re = 3000$ to other values of Re for streamwise independent disturbances. From the definition of B in Eq. (10), B is proportional to the ratio r_0/d. It is clear that small and large B correspond to the wide-gap and narrow-gap cases, respectively. In our results, we choose $B = 0.05$, 0.5, 2, and 20. $B = 0.05$ is a wide-gap case, $B = 0.5$ and 2 are two medium-gap cases, and $B = 20$ is a narrow-gap case.

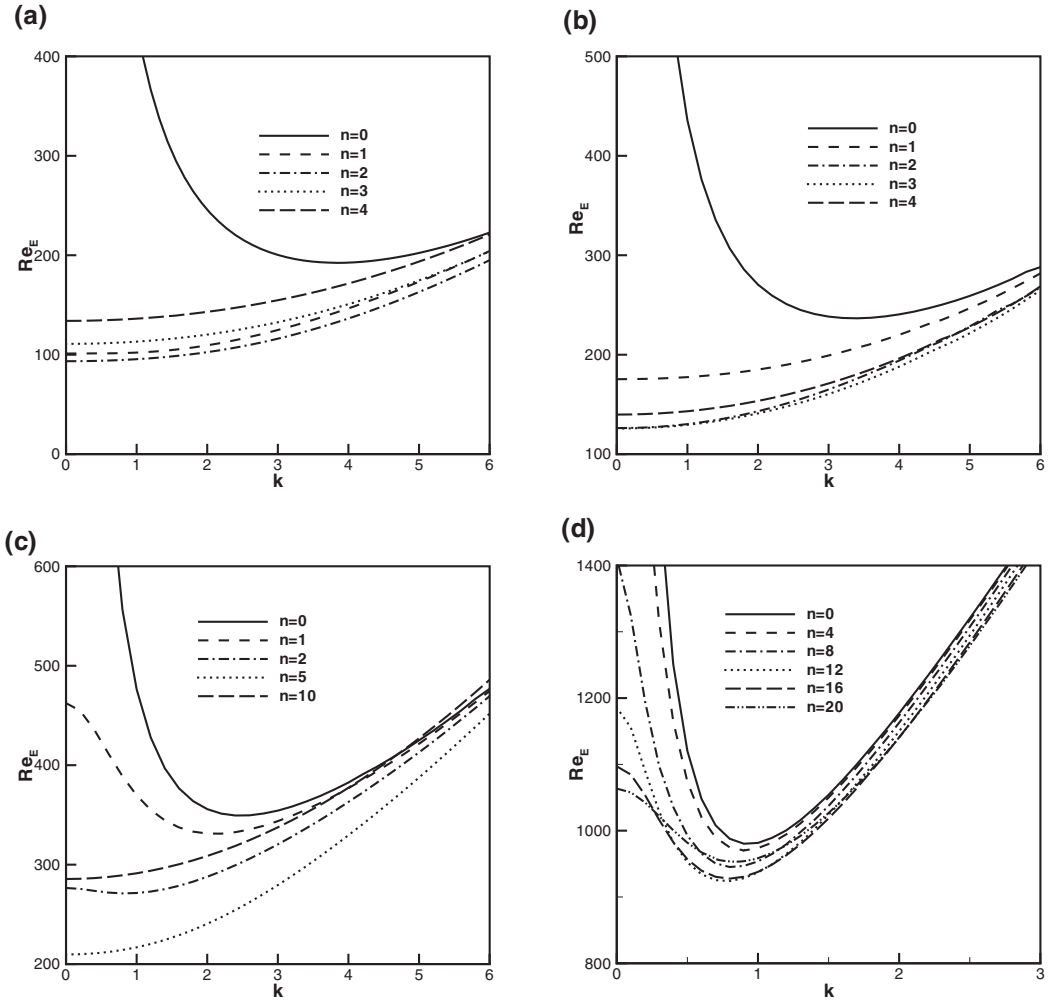

FIG. 2. The curves of the critical energy Reynolds number Re_E versus the streamwise wavenumber k for various B. (a) $B = 0.05$, (b) $B = 0.5$, (c) $B = 2$, (d) $B = 20$.

A. Condition for no energy growth

In this subsection, we are interested in the condition for which there is no growth of the perturbation kinetic energy. Energy methods give conditions for no energy growth. For a linear system $\frac{\mathrm{d}}{\mathrm{d}t}\mathbf{x} = -i\mathscr{L}\mathbf{x}$, we define the energy density $\mathscr{E} = \| \mathbf{x} \|_2^2$. There is no energy growth if and only if all the eigenvalues of the anti-symmetric part of $\mathscr{L}$, i.e., $\frac{1}{2}(\mathscr{L} - \mathscr{L}^H)$ in which H denotes the Hermitian transpose, lie in the lower half plane. For hydrodynamics stability problems, the linear stability theory gives the sufficient conditions for instability, and the energy theory gives the sufficient conditions for stability. The energy method shows that there is no energy growth if the Reynolds number is less than the critical energy Reynolds number Re_E.

We now examine the condition below which the kinetic energy of an infinitesimal disturbance decays monotonically. Let σ be the leading eigenvalue of $\frac{1}{2}(\mathscr{L} - \mathscr{L}^H)$. The condition with no energy growth is given by the energy Reynolds number Re_E such that $\sigma = 0$. For a given Bingham number B, the global critical energy Reynolds number is given by $Re_g = \min_{n,k} Re(n, k)$, in which $\sigma(n, k, B, Re) = 0$.

In Fig. 2, we plot the curves of the critical energy Reynolds number versus the streamwise wavenumber for various azimuthal wavenumbers at some typical values of $B = 0.05$, 0.5, 2, and 20. $B = 0.05$ and 20 are close to the wide-gap limit of $r^* \to 0$ and the narrow-gap limit of $r^* \to \infty$.

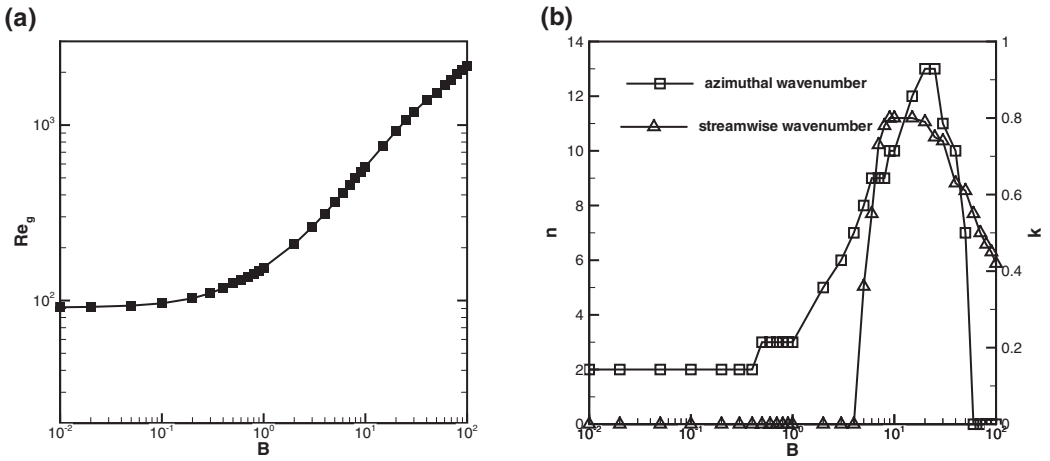

FIG. 3. Global critical energy Reynolds number Re_g versus the Bingham number B.

In Fig. 2(a) for $B = 0.05$, for the axisymmetric case of $n = 0$ the minimal critical energy Reynolds number is about 200 at $k \approx 4$. For non-axisymmetric cases of $n > 0$, the critical Reynolds number increases with the streamwise wavenumber k. The lowest critical energy Reynolds number of $Re \simeq 93.5$ is achieved at the longwave limit of $k = 0$ by the disturbance of $n = 2$. For $n \geq 2$, with the increase of n the energy stability curves become more stable at all streamwise wavenumbers. In the limit of zero yield stress, one recovers a Newtonian pipe Poiseuille flow. In this case, the velocity profile of the base state of Bingham-Hagen-Poiseuille flow approaches the Newtonian case. However, as $B \to 0$ the linear stability problem of Bingham-Hagen-Poiseuille flow cannot reduce to the Newtonian one because of additional boundary conditions arising from the perturbation of the yielded surface. For Hagen-Poiseuille flow of a Newtonian fluid, the global lowest energy Reynolds number of $Re \simeq 81.6$ is associated with non-axisymmetric and streamwise dependent disturbances with $n = 1$ and $k \simeq 1.1$.[4] However, for Bingham-Hagen-Poiseuille flow as $B \to 0$ the most unstable disturbance is associated with the streamwise uniform and non-axisymmetric disturbances with $n = 2$.

In Fig. 2(b), the curves of the critical energy Reynolds number are plotted for a medium-gap case of $B = 0.5$. In this figure, the structures of the curves of both the axisymmetric and the non-axisymmetric cases are similar to those of $B = 0.05$ in Fig. 2(a). For $B = 0.5$, the disturbance with $n = 3$ has the lowest critical energy Reynolds number of $Re \simeq 125.8$ at $k = 0$. For $n \geq 3$, the critical energy Reynolds number increases with n at all k. In Fig. 2(c), the curves of the critical energy Reynolds are plotted for a narrower-gap case of $B = 2$. In this figure, the lowest critical energy Reynolds number of $Re \simeq 209.7$ is given by the disturbance of $n = 5$ at $k = 0$. For $n \geq 5$, the minimum value of each curves occurs at $k = 0$ and the critical energy Reynolds number increases with n at all k. For $n < 5$, the flow becomes more unstable with the increase of n at all k. Being different from the curves of non-axisymmetric cases in Figs. 2(a) and 2(b), in Fig. 2(c) for $n = 1$ and 2 the streamwise wavenumber of the most unstable mode is non-zero. In Fig. 2(d), the curves of the critical energy Reynolds number are plotted for the narrow-gap case of $B = 20$. In this figure, the lowest critical energy Reynolds number of each curve is achieved by a streamwise non-uniform disturbance. The global lowest energy Reynolds number is associated with non-axisymmetric and streamwise dependent disturbances with $n = 12$ and $k \simeq 0.8$. It is interesting to consider the narrow-gap case of $B \to \infty$. As $B \to \infty$, substituting $n/r \sim \beta$ and $1/r \to 0$ into Eqs. (23)–(26), where β is the spanwise wavenumber, the present problem reduces to the controlling equations for the plane Bingham Poiseuille flow.[22]

In order to know the effect of B on the energy stability of the Bingham-Hagen-Poiseuille flow, we plot in Fig. 3(a) the curve of Re_g as a function of B, and in Fig. 3(b) the azimuthal wavenumber and the streamwise wavenumber corresponding to the critical energy Reynolds number. At small Bingham numbers, Re_g slightly increases with B. At large Bingham numbers $B \geq 30$, Re_g increases

with B at the order of $Re_g \sim O(B^{1/2})$, which is consistent to the results of plane Bingham Poiseuille flow.[22] In Fig. 3(b), for $B < 4$ the most unstable disturbance is in the form of streamwise independent streaks ($k = 0$). For $B > 4$, the streamwise wavenumber of the critical mode reaches the maximal value at about $B \sim 10$. For large B, k decreases with the increase of B. At small $B < 0.4$, the azimuthal wavenumber n is 2. With the increase of B, n increase to 13 at $B \approx 30$. As B increases further, n decrease to 0 for $B > 60$. For small $B < 4$, the critical mode is in the form of streamwise independent vortices. For medium $4 < B < 60$, the critical mode is oblique. For large $B > 60$, the critical mode is azimuthal uniform.

From Eq. (5), the viscosity of a Bingham fluid decreases with the increase of $\dot{\gamma}$. This shows that the Bingham fluid is shear-thinning. It is interesting to compare the stability of Hagen-Poiseuille flow of a Bingham fluid with other types of shear-thinning fluids. Recently, Liu and Liu[31] studied the linear stability of Hagen-Poiseuille flow of a shear-thinning fluid. The non-Newtonian viscosity is described by the Carreau rheological law. The energy analysis showed that the non-axisymmetric disturbance with the azimuthal wavenumber $n = 1$ has the lowest critical energy Reynolds number at a finite streamwise wavenumber k for both the Newtonian and shear-thinning cases. For Bingham-Hagen-Poiseuille flow, the azimuthal wavenumber of the most unstable mode changes with the increase of B.

B. Transient behavior and non-modal stability

In the non-modal theory, two types of problems are of particular interest, i.e., response to external excitations and transient energy growth of initial conditions. For the former, the norm of the resolvent denotes the maximum amplification of external excitations; for the latter, the growth function $G(t)$ identifies the optimal growth of energy at time t.

1. Pseudospectrum and response to external excitations

The behavior of a non-normal operator depends on not solely the eigenvalues, but the structure of ϵ-pseudospectra. As discussed in Sec. III, the resolvent norm represents the amplification of response to external forcing. In order to know the response to external excitations, we plot the ϵ-pseudospectra for several typical parameters.

We have computed the eigenvalue problem for a wide range of Reynolds and Bingham numbers. The computational results show that all the eigenvalues are stable. In Fig. 4, the ϵ-pseudospectra and the spectrum are plotted for streamwise non-uniform disturbances at $Re = 3000$ for the cases of $B = 0.05$ and 20. For plane and pipe Poiseuille flows, the eigenvalues are located on three main branches, called A, P, and S.[32] In Fig. 4, being similar to the Newtonian one, the spectrum of Bingham-Hagen-Poiseuille flow also consists of three main branches. The eigenvalues on the left branch, the right branch, and the middle branch are A, P, and S modes. A modes, which have largest variation close to the wall, have rather small phase velocities, whereas, the P modes, which have their maxima close to the surface of the unyielded zone, have much higher phase speeds. The S modes, which are highly damped, have a phase speed ($c_r = \omega_r/k$) that is nearly equal to 2/3. Being different from the Newtonian pipe Poiseuille flow, the S branch consists of spectra locating in two straight lines because the eigenvalues of the Squire mode depart from the Orr-Sommerfeld modes in the S branch. As shown in Figs. 4(a) and 4(b) for $B = 0.05$, the eigenvalues of Squire mode only slightly depart from the Orr-Sommerfeld modes. As B increase to 20, in Figs. 4(c) and 4(f) the distance between the phase speeds of these two modes increases. Comparing Figs. 4(c) and 4(d) with 4(a) and 4(b), we found that with the decrease of B, the number of the eigenvalues of the A, P, and S branches increases.

In Fig. 5, we plot the spectrum and ϵ-pseudospectra for streamwise uniform disturbances for $B = 0.05$ and $B = 20$. In these two figures, the structures of the pseudospectrum and eigenvalues are qualitatively similar to the Squire mode of the Newtonian pipe Poiseuille flow. In Figs. 4 and 5, it is found that the numerical range protrudes into the upper plane. This means that at the initial time the energy of the disturbance is growing. Comparing Figs. 5(a) and 5(b) shows that the numerical range protrudes deeper into the upper plane for $B = 0.05$ than for $B = 20$. This result shows that the initial energy growth rate decreases with the increase of B.

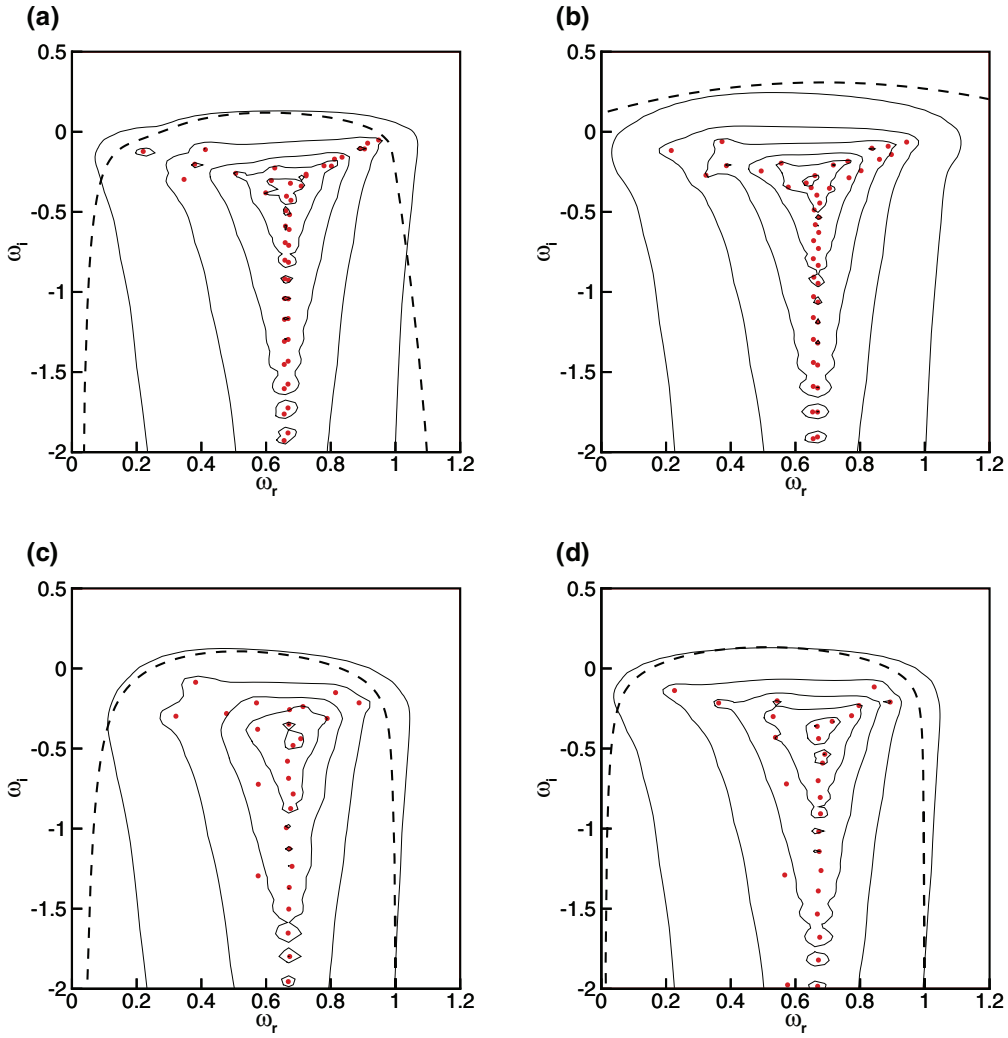

FIG. 4. Spectrum and pseudospectra for streamwise non-uniform disturbances in Bingham-Hagen-Poiseuille flow at $Re = 3000$. (a) $n = 0$, $k = 1$, $B = 0.05$, (b) $n = 1$, $k = 1$, $B = 0.05$, (c) $n = 0$, $k = 1$, $B = 20$, (d) $n = 12$, $k = 1$, $B = 20$. •, eigenvalues; dashed line $--$ $-$, boundary of the numerical range; solid lines $-$, contours from outermost to innermost (ith) represent levels of the ϵ-pseudospectrum from $\epsilon = 10^{-1}$ to 10^{-i} .

In the complex ω plane, we are particularly interested in the resonance of the real axis because it corresponds to external excitations at real frequencies. In Fig. 6, we plot the maximum response to spatially harmonic forcing at a wide range of frequencies for several typical cases at $Re = 3000$. In Figs. 6(a)–6(d), the curves of the response of the streamwise uniform disturbances are plotted for various Bingham numbers. In each figure, the disturbance is mainly amplified in the low frequency range and decreases significantly in the high frequency range. At $B = 0.05$, 0.5, and 2, the azimuthal wavenumbers of the most amplified streamwise mode are $n = 1$, 2, and 3. However, we found it interesting that for a large Bingham number of $B = 20$ the azimuthal wavenumber of the most amplified mode is $n = 1$. For $B = 0.05$, the azimuthal wavenumber of the most amplified mode is the same as the Newtonian pipe flow. But the amplification in Fig. 6(a) for $B = 0.05$ is lower than the Newtonian case in which $\mathcal{R}(0)$ of $n = 1$ is more than 10^4.[31]

In Figs. 6(e) and 6(f), the curves of the response of disturbance in the form of oblique waves with $k = 1.0$ and various n are presented for $B = 0.05$ and 20. In these two figures, most of the curves show that external forcing is significantly amplified in a limited band of frequency. As shown in Fig. 4, the intersection region of A, P, S branches is very sensitive to disturbances. The inner

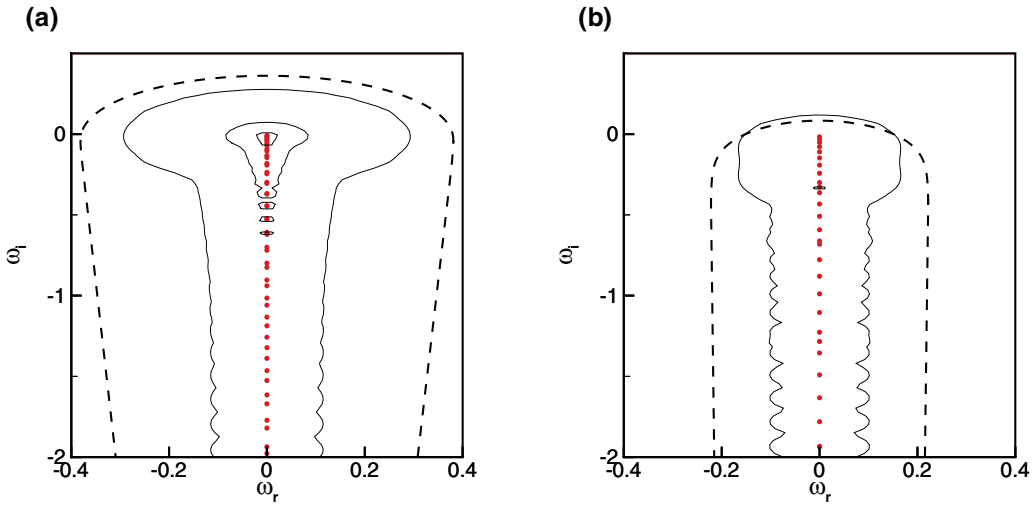

FIG. 5. Spectrum and pseudospectra for streamwise uniform disturbances in Bingham-Hagen-Poiseuille flow at $Re = 3000$. (a) $n = 2$, $k = 0$, $B = 0.05$, (b) $n = 15$, $k = 0$, $B = 20$. •, eigenvalues; dashed line $--$, boundary of the numerical range; solid lines $-$, contours from outermost to innermost (ith) represent levels of the ϵ-pseudospectrum from $\epsilon = 10^{-1}$ to 10^{-i}.

region of the plateau shape is mainly due to the resonance between the intersection region and disturbances (off-resonance), and the boundary region is mainly due to the resonance of the left and right branches (at resonance). Comparing Fig. 6(e) with 6(a) and 6(f) with 6(b) shows that the maximum amplification of the streamwise uniform forcing is much higher than the streamwise dependent case.

Fig. 6 shows the frequency of the most amplified disturbance changes with the streamwise wavenumber. In order to know the maximum response to forcing with different streamwise wavenumbers, we define

$$\mathcal{R}_{max} = \max \mathcal{R}(\omega). \tag{51}$$

In Fig. 7, we plot the curves of the maximum response of $\mathcal{R}_{max}$ versus the streamwise wavenumber k for different Bingham numbers at $Re = 3000$. As shown in these figures, the maximum energy growth is always realized at $k = 0$. In Figs. 7(a)–7(c) for $B = 0.05$, 0.5, and 2, the maximum response $\mathcal{R}_{max}$ of each curve decreases with the increase of k. For $B = 0.05$, 0.5, and 2, the azimuthal wavenumber of the most amplified mode is $n = 1$, 2, and 3. As shown in Fig. 7(d) for $B = 20$, the maximum response of $n = 0$ and 1 does not decrease monotonically with k, and the largest response is achieved by the mode with $n = 1$ at $k = 0$.

In order to find the azimuthal wavenumber of the most amplified external forcing, in Fig. 8 we plot the curves of the maximum response $\mathcal{R}_{max}$ versus the Bingham number B for various n at $Re = 3000$. In Fig. 8, in the range of $B < 0.3$, $\mathcal{R}_{max}$ of $n = 1$ gradually decreases with the increase of B, and $\mathcal{R}_{max}$ of other modes is insensitive to B. For $B < 0.3$, the value of $\mathcal{R}_{max}$ of $n = 1$ is higher than the values of other curves. As B increases further, $\mathcal{R}_{max}$ of each curve becomes more sensitive to B and decreases drastically with the increase of B. For $0.3 < B < 0.8$, $n = 2$ or $n = 3$ becomes the most amplified mode. It is interesting that for large B the value of $\mathcal{R}_{max}$ of $n = 1$ almost does not change with B, and the disturbance with $n = 1$ becomes the most amplified mode.

In order to know more about the physical mechanism of the response to external forcing, we present the spatial structures of the optimal input of spatially harmonic forcing and the output for $B = 0.05$, 0.5, and 2 at $Re = 3000$ in Fig. 9. As the optimal frequency is $\omega = 0$, only plots of input and output are needed. We have computed the velocity fields of the optimal input and output. The result shows that the streamwise velocity components of the input disturbances are very weak and the radial and azimuthal velocity components have most of the perturbation kinetic energy. For the optimal output, the magnitudes of radial and azimuthal velocity components are smaller in comparison with the streamwise component. For $B = 0.05$, 0.5, and 2, the azimuthal wavenumber

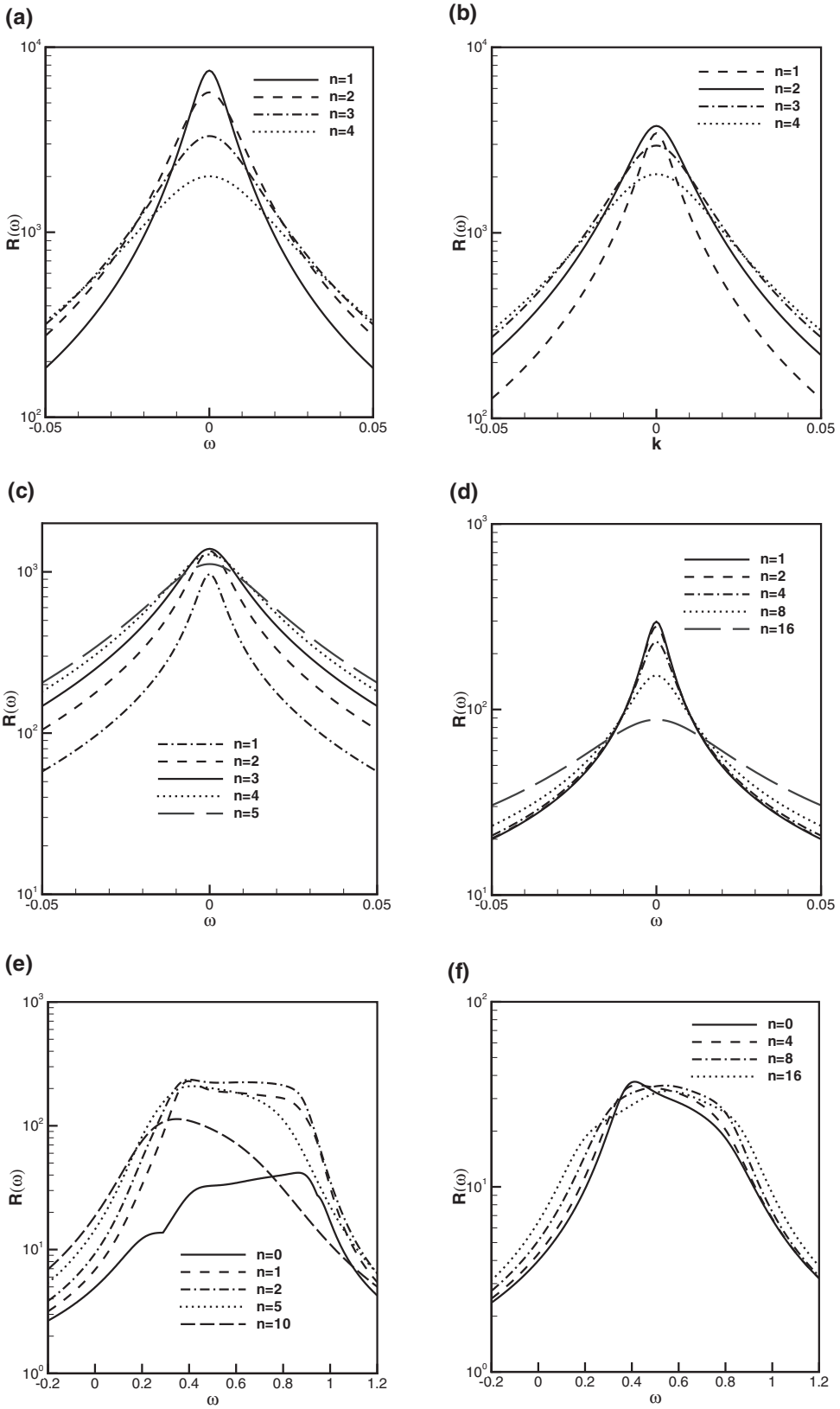

FIG. 6. The curves of the optimal response $\mathcal{R}(\omega)$ to spatially harmonic external forcing versus the real frequency ω at $Re = 3000$. (a) $k = 0$, $B = 0.05$, (b) $k = 0$, $B = 0.5$, (c) $k = 0$, $B = 2$, (d) $k = 0$, $B = 20$, (e) $k = 1$, $B = 0.05$, (f) $k = 1$, $B = 20$.

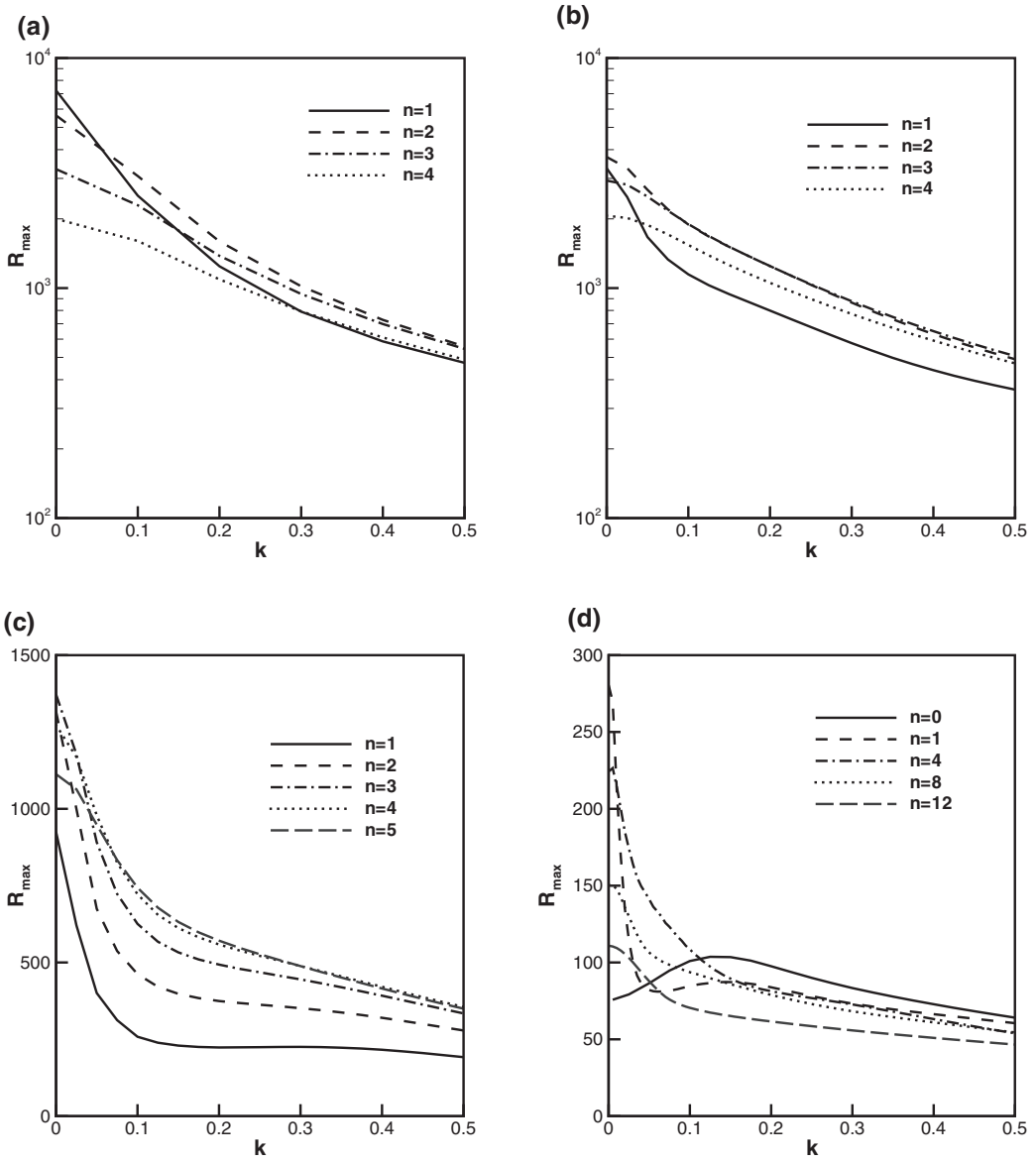

FIG. 7. The curves of the maximum response $\mathcal{R}_{max}$ to spatially harmonic external forcing versus the wavenumber k at $Re = 3000$. (a) $B = 0.05$, (b) $B = 0.5$, (c) $B = 2$, (d) $B = 20$.

of the most amplified disturbance is $n = 1$, 2, and 3. The velocity field $u\mathbf{e}_r + v\mathbf{e}_\theta$ associated with the optimal input is plotted in Figs. 9(a), 9(c), and 9(e) for $B = 0.05$, 0.5, and 2. The flow of the input field is characterized by pairs of counter-rotating vortices. The optimal output of the amplitude of the streamwise velocity component w plotted in Figs. 9(b), 9(d), and 9(f) shows that the counter-rotating vortices of the input result in streaks of output. The flow fields of the optimal input and output in Fig. 9 imply that the lift-up effect is responsible for the amplification of the optimal input.

2. Transient growth and optimal disturbances

In this subsection, we will study the transient energy growth of the optimal disturbance in the form of response to initial conditions. The aim is to provide physical insights into the transition from laminar flow towards turbulence in Bingham-Hagen-Poiseuille flow. In plane channel and pipe flows, one possible path from laminar to turbulence is the SV scenario in which transition is initiated

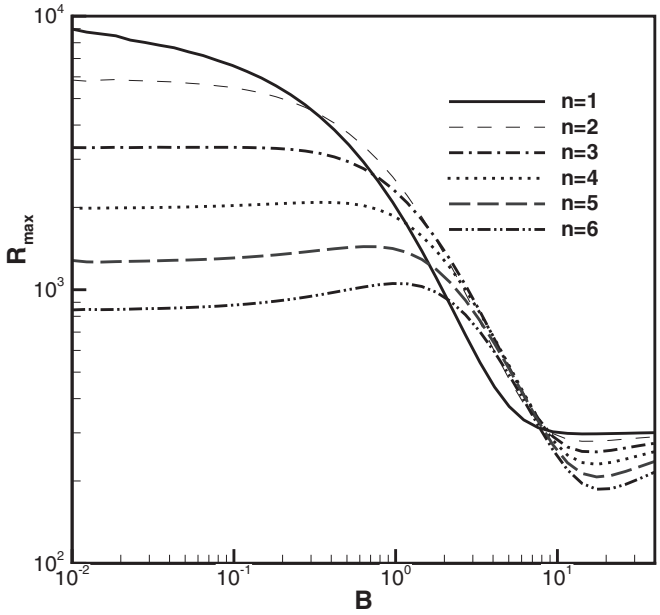

FIG. 8. The curves of the maximum response $\mathcal{R}_{max}$ versus the Bingham number B.

by optimal streamwise vortices. Schematically, the SV scenario is

(SV) streamwise vortices $\Rightarrow$ streamwise streaks $\Rightarrow$ streak breakdown $\Rightarrow$ transition.

This scenario was shown to be pertinent in parallel shear flows, such as plane Couette and plan Poiseuille flows,[17] and boundary layers.[32] The optimal perturbations in the form of two-dimensional

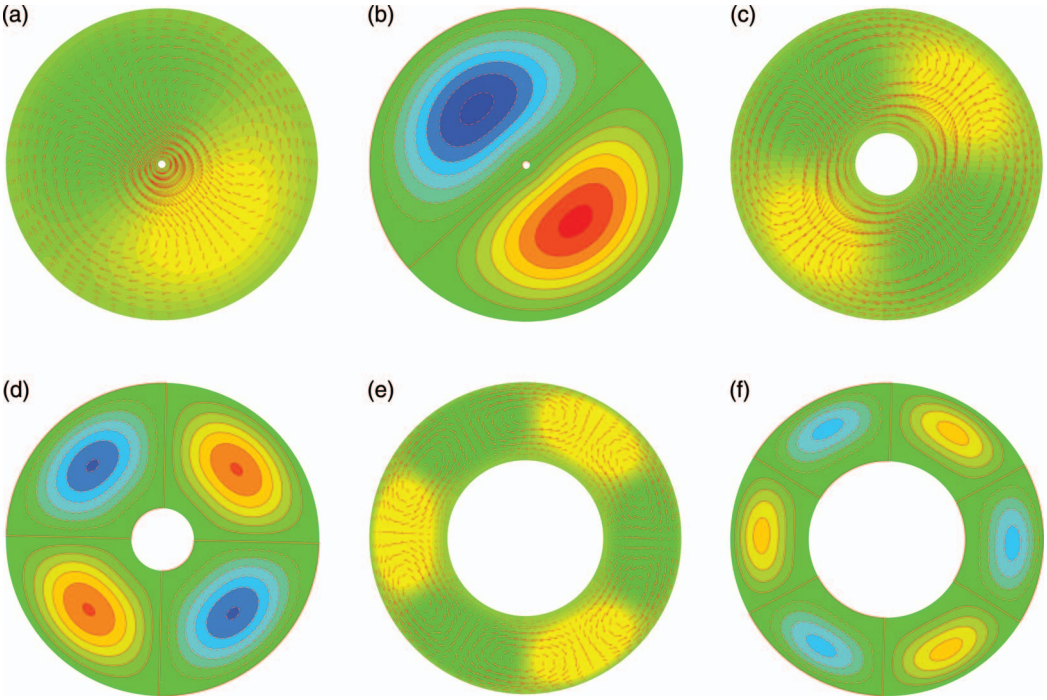

FIG. 9. Cross-stream (r-θ) view of the optimal input and output flow fields of the response to spatially harmonic forcing at $Re = 3000$. (a), (c), and (e): The velocity components of u and v of the input. (b), (d), and (f): Isolines of the velocity component w of the output. (a) and (b) $B = 0.05$ and $n = 1$; (c) and (d) $B = 0.5$ and $n = 2$; (e) and (f) $B = 2$ and $n = 3$.

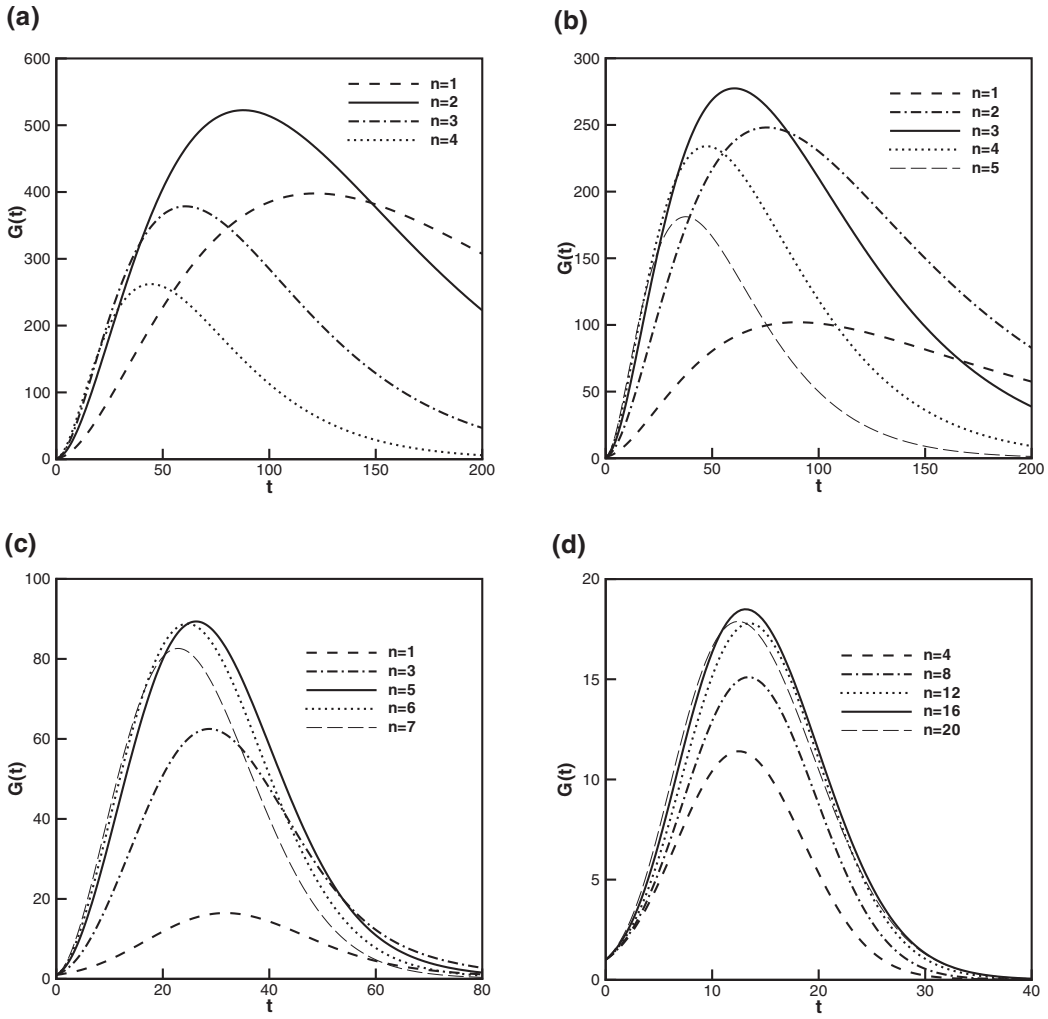

FIG. 10. The curves of transient energy growth function $G(t)$ versus time t for various azimuthal wavenumbers. (a) $B = 0.05$, $Re = 3000$, (b) $B = 0.5$, $Re = 3000$, (c) $B = 2$ $Re = 3000$, (d) $B = 20$ $Re = 6000$.

streamwise rolls evolve into streamwise streaks via the lift up mechanism. The amplification of the optimal disturbances can be sufficiently large that the disturbances may result in the modification of the basic flow rendering it unstable to three-dimensional perturbations. This secondary instability, also referred to as streak breakdown, leads to turbulence. The mechanism of the transient growth is responsible for the formation of streaks.

We can define the energy growth maximized over time as

$$G_{max} = G(t_{opt}) = \max G(t), t \geq 0. \tag{52}$$

If the Reynolds number is less than the critical energy Reynolds number Re_g, then $G(t) \leq 1$ for all time. In this case, $G_{max} = 1$ and $t_{opt} = 0$. If the Reynolds number exceeds the linear critical Reynolds number Re_c such that the operator $\mathscr{L}$ has an unstable eigenvalue, then $G_{max} \to \infty$ at $t_{opt} \to \infty$. If $Re_g < Re < Re_c$, the flow is linearly stable but has a transient energy growth. For Bingham-Hagen-Poiseuille flow, Re_c is infinite. When examining the characteristics of the transient growth, we only need to consider the case of $Re > Re_g$.

In Fig. 10, the curves of maximum response to initial conditions are plotted for streamwise uniform disturbances with various azimuthal wavenumbers for different B. In Fig. 10, each curve shows that the disturbance experiences a rapid transient growth and then decays after t_{opt} because of

the effect of viscosity. Being similar to Newtonian plane and pipe Poiseuille flows, for streamwise uniform disturbances the lift up effect is responsible for the energy growth.[15,16] For the Newtonian pipe Poiseuille flow, the optimal energy growth is achieved by the streamwise uniform disturbance with $n = 1$.[17] At $Re = 3000$, the optimal energy growth of Hagen-Poiseuille flow is $G_{max} \approx 649.1$ at a specific time $t_{opt} \approx 148.5$. However, as shown in Fig. 10(a) for $B = 0.05$ the optimal energy growth of $G_{max} \approx 522.5$ is achieved by the disturbance with $n = 2$ at a specific time $t_{opt} \approx 87.6$. This result shows that as $B \to 0$, the optimal energy growth of Bingham-Hagen-Poiseuille flow is lower than Hagen-Poiseuille flow because of the presence of an unyielded zone. In Fig. 10(a), the disturbances of the modes of $n = 3$ and 4 reach the maximum energy growth more rapidly than the mode of $n = 2$. The energy growth of the optimal mode with $n = 1$ is lower than that of $n = 2$, but the optimal time t_{opt} of $n = 1$ is larger than that of $n = 2$. After the optimal time, it is found that the energy growth of the mode with $n = 1$ damps more slowly than all other modes.

In Fig. 10(b) for $B = 0.5$, the optimal energy growth of $G_{max} \approx 277.4$ is achieved by the disturbance with $n = 3$ at $t_{opt} \approx 60.2$. For $n < 3$, the energy growth of the optimal disturbance damps more slowly than $n = 3$. For $n > 3$, both the optimal energy growth G_{max} and the optimal time t_{opt} decrease with the increase of n. With the increase of B, the azimuthal wavenumber n of the optimal disturbance increases. In Figs. 10(c) and 10(d), for $B = 2$ and 20 the azimuthal wavenumbers of the optimal disturbances are $n = 5$ and 16, respectively.

In order to know the optimal energy growth for streamwise non-uniform disturbances, we plot the curves of G_{max} versus the streamwise wavenumber k for different Bingham numbers. In Figs. 11(a) and 11(b) for $B = 0.05$ and 0.5, the maximum energy growth of each curve is realized at $k = 0$ and G_{max} decreases with the increase of k. This means at small Bingham numbers the optimal disturbances are in the form of streamwise uniform vortices and streaks. In Figs. 11(c) and 11(d) for $B = 2$ and 20, the maximum energy growth of each curve is achieved by a disturbance with a non-zero streamwise wavenumber. This result means that for large Bingham numbers, the optimal disturbances are in the form of oblique waves.

In Fig. 12, we plot the maximum energy growth and the corresponding streamwise and azimuthal wavenumbers of the optimal disturbance versus the Bingham number. In Fig. 12(a), for small values of $B \leq 0.1$, G_{max} slightly decreases with the increase of B. For medium value of $0.1 < B \leq 1$, G_{max} becomes more sensitive to B and gradually decreases with the increase of B. For sufficiently large values of $B > 1$, it is found that the maximum energy growth behaves closely as $G_{max} \sim B^{-1}$. In Fig. 12(b), it is found that the azimuthal wavenumber of the optimal disturbance increases with B. The reason is that the radial size and the azimuthal size of the input vortices and output streaks should be comparable for all B. For large Bingham numbers, we speculate that the BHPF behaves like the PBPF. We can link the azimuthal wavenumber of the optimal disturbance of BHPF to PBPF. For BHPF, the azimuthal wavenumber of the optimal response to initial conditions can be estimated by $n \approx (2B + 1)\beta/2$, in which β is the spanwise wavenumber of optimal disturbance for PBPF. For BHPF, the azimuthal wavenumber of the optimal disturbance is $n = 5$ at $B = 2$. The estimated value of spanwise wavelength is 3.33 for BHPF. This result is very close to the result for PBPF in which $\beta \approx 3.11$ at $B = 2$.[22] In Fig. 12(b), in the range of $B < 1$ the streamwise wavenumber of the optimal disturbance is zero. In this case, the optimal disturbances are in the form of streamwise uniform vortices and streaks. For medium values of $1 < B < 10$, the streamwise wavenumber k of the optimal disturbance increases with the increase of B. For sufficiently large value of B, the streamwise wavenumber k of the optimal disturbance is close to 1.4. For $B > 1$, the optimal disturbances are in the form of oblique waves.

In Fig. 13, we plot the flow fields of the optimal disturbance at the initial time $t = 0$ and the optimal time $t = t_{opt}$ for different Bingham numbers. In Figs. 13(a)–13(d) for $B = 0.05$ and 0.5, at the initial time $t = 0$ and the optimal time $t = t_{opt}$, the flow fields are characterized by two counter-rotating vortices and streaks. These flow structures of the initial problem are very similar to that of the input-output problem in Fig. 9. The lift up effect is responsible for the energy growth of the streamwise uniform disturbance. In Figs. 13(e) and 13(f) for $B = 2$, the flow fields are in the form of oblique streaks. For streamwise dependent disturbances, both the lift up effect and the two-dimensional Reynolds stress mechanism[33] are responsible for the transient growth of the disturbances.

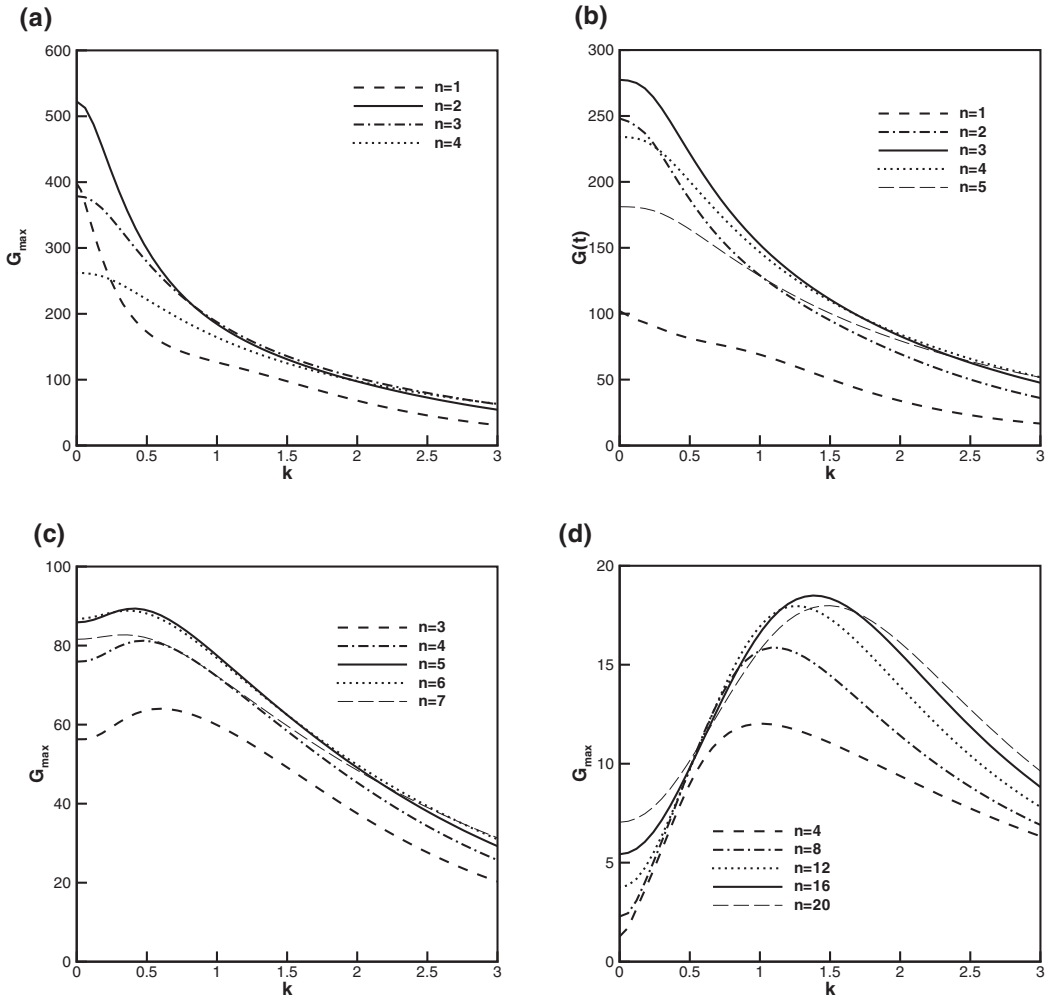

FIG. 11. The maximum transient energy growth G_{max} versus the streamwise wavenumber k. (a) $B = 0.05$, $Re = 3000$, (b) $B = 0.5$, $Re = 3000$, (c) $B = 2$, $Re = 3000$, (d) $B = 20$, $Re = 6000$.

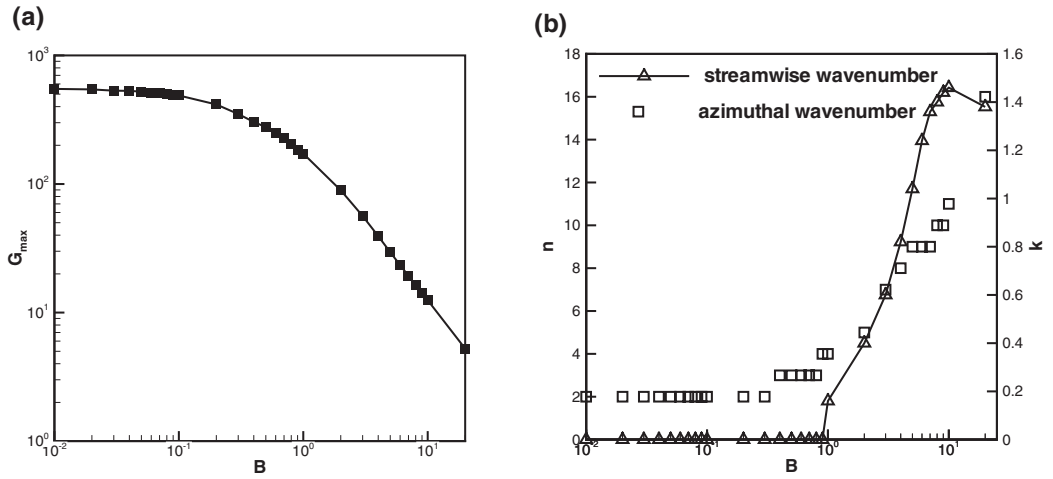

FIG. 12. (a) The maximum transient energy growth G_{max} and (b) corresponding azimuthal and streamwise wavenumbers versus the Bingham number B at $Re = 3000$.

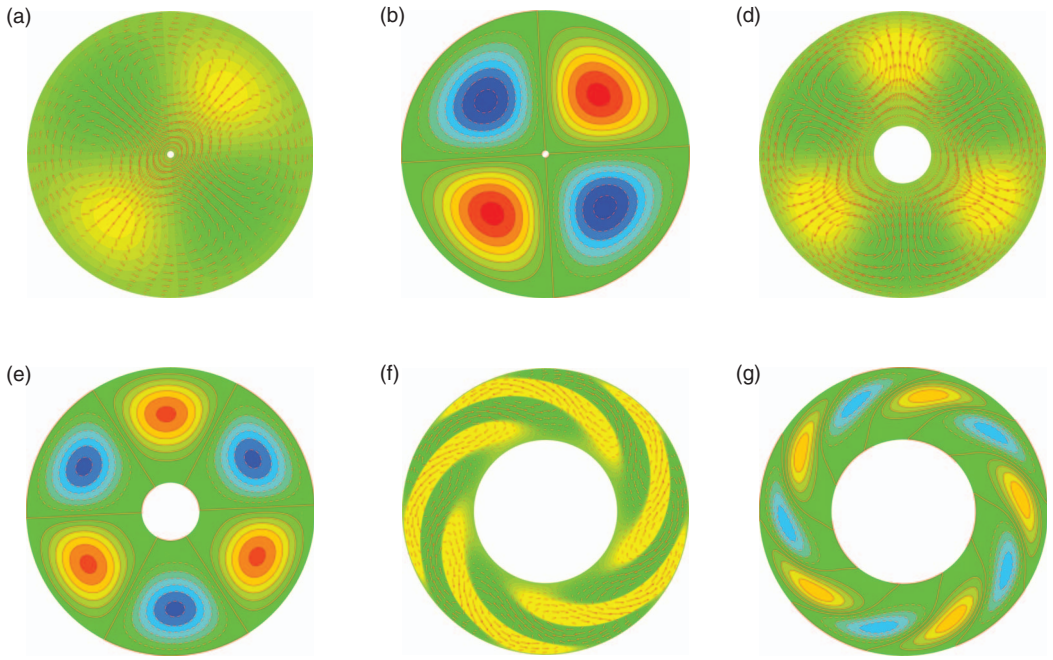

FIG. 13. The cross-stream (r-θ) view of the optimal input and output flow fields of the response to initial conditions at $Re = 3000$. (a), (c), and (e): The velocity components of u and v of the input. (b), (d), and (f): Isolines of the velocity component w of the output. (a) and (b) $B = 0.05$ and $n = 2$; (c) and (d) $B = 0.5$ and $n = 3$; (e) and (f) $B = 2$ and $n = 5$.

For the problem of response to external forcing, the optimal disturbance is always in the form of streamwise uniform streaks. The azimuthal wavenumber of the optimal disturbance can be $n = 1$, 2, and 3. However, for the problem of response to initial conditions, for large Bingham numbers the optimal disturbances are in the form of oblique waves. The azimuthal wavenumber of the optimal disturbance increases with B.

V. CONCLUSIONS

In the present paper, we have investigated the linear stability in Bingham-Hagen-Poiseuille flow using the energy method and the non-modal stability theory. We focus on the effect of yield stress on the stability of the flow.

We investigated the critical condition of the energy Reynolds number Re_E below which there is no energy growth for both axisymmetric and non-axisymmetric disturbances. The results of energy stability analysis show that both axisymmetric and non-axisymmetric disturbances can experience an energy growth at the initial time. For small Bingham numbers, the critical condition is determined by a streamwise uniform disturbance. For sufficiently large values of the Bingham number, it is determined by a streamwise non-uniform disturbance. As $B \to 0$, the critical condition is reached by the mode with the azimuthal wavenumber $n = 2$ and the streamwise wavenumber $k = 0$. This result is different from the Newtonian pipe Poiseuille flow in which the global lowest energy Reynolds number is associated with the non-axisymmetric disturbance with the wavenumbers of $n = 1$ and $k \neq 0$. It is found that the global critical energy Reynolds number Re_g increases with the increase of B. At sufficiently large Bingham numbers, the global critical energy Reynolds number behaves closely as $Re_g \sim B^{1/2}$.

In the non-modal stability analysis, we focus on the response to external excitations and initial conditions. The response to external excitations is characterized by the ϵ-pseudospectrum. For Bingham-Hagen-Poiseuille flow, both axisymmetric and non-axisymmetric external forcing can be amplified by a rather large factor. However, the amplification of response to axisymmetric external forcing is much lower than that of the non-axisymmetric one. The most amplified forcing is always

in the form of streamwise uniform vortices at the frequency of $\omega = 0$. For $B < 1$, the maximum amplification decreases with the increase of B. For sufficiently large B, the maximum amplification becomes insensitive to B. For small B, the azimuthal wavenumber of the most amplified mode is $n = 1$. For $B < 1$, with the increase of B the azimuthal wavenumber of the most amplified mode can increase to $n = 2$ or 3. As B exceeds 1, the azimuthal wavenumber of most amplified mode is always $n = 1$.

We have studied the transient energy growth of the optimal disturbance in the form of initial conditions. The results show that even though all the eigenvalues of Bingham-Hagen-Poiseuille flow are stable, the disturbances also can be amplified substantially. For small B, the optimal transient energy growth is achieved by streamwise uniform vortices and streaks. The lift up effect is responsible for the transient energy growth. For sufficiently large B, the optimal disturbance is in the form of oblique waves. Both the lift up effect and the two-dimensional Reynolds stress mechanism are responsible for the transient energy growth. At small B, the maximum value of the optimal transient energy growth G_{max} slightly decreases with the increase of B. At large B, G_{max} decreases as the order of B^{-1}. With the increase of B, the azimuthal wavenumber of the optimal disturbance increases. The azimuthal wavenumber of the optimal disturbance can be estimated by $n \approx (2B + 1)\beta/2$, in which β is the spanwise wavenumber of optimal disturbance for the plane Bingham-Poiseuille flow.

We also compared results of the case of $B = 0.05$ to the Hagen-Poiseuille flow. The result shows that as $B \to 0$ Bingham-Hagen-Poiseuille flow is more stable than Hagen-Poiseuille flow for both the energy stability and non-modal stability problems. Moreover, the azimuthal wavenumbers of the optimal disturbance in the form of initial conditions are different for these two cases.

ACKNOWLEDGMENTS

This work was supported by National Natural Science Foundation of China (NNSFC) (Grant Nos. 11102211, 50890182, and 11072249) and the Knowledge Innovation Program of Chinese Academy of Sciences (CAS) (KGCX-SW-409).

[1] R. Byron-Bird , G. C. Dai, and B. J. Yarusso, "The rheology and flow of viscoplastic materials," Rev. Chem. Eng. **1**, 1–70 (1983).
[2] R. P. Chhabra and J. F. Richardson, *Non-Newtonian Flow and Applied Rheology: Engineering Applications*, 2nd ed. (Elsevier, Oxford, 2008).
[3] O. Reynolds, "An experimental investigation of the circumstances which determine whether the motion of water shall be direct or sinuous and of the law of resistance in parallel channels," Proc. R. Soc. London **35**, 84–99 (1883).
[4] P. J. Schimid and D. S. Henningson, "Optimal energy density growth in Hagen-Poiseuille flow," J. Fluid Mech. **277**, 197–225 (1994).
[5] A. Meseguer and L. N. Trefethen, "Linearized pipe flow to Reynolds number 10^7," J. Comput. Phys. **186**, 178–197 (2003).
[6] B. Hof, C. W. H. van Doorne, J. Westerweel, F. T. M. Nieuwstadt, H. Faisst, B. Eckhardt, H. Wedin, R. R. Kerswell, and F. Waleffe, "Experimental observation of nonlinear traveling waves in turbulent pipe flow," Science **305**, 1594–1598 (2004).
[7] J. Peixinho and T. Mullin "Decay of turbulence in pipe flow," Phys. Rev. Lett. **96**, 094501 (2006).
[8] R. R. Kerswell, "Recent progress in understanding the transition to turbulence in a pipe," Nonlinearity **18**, R17–R44 (2005).
[9] B. Eckhardt, T. Schneider, B. Hof, and J. Westerweel, "Turbulence transition in pipe flow," Annu. Rev. Fluid Mech. **39**, 447–468 (2007).
[10] L. N. Trefethen, A. E. Trefethen, S. C. Reddy, and T. A. Driscoll, "Hydrodynamics stability without eigenvalues," Science **261**, 578–584 (1993).
[11] S. Reddy and D. S. Henningson, "Energy growth in viscous channel flows," J. Fluid Mech. **252**, 209–238 (1993).
[12] P. J. Schmid, "Nonmodal stability theory," Annu. Rev. Fluid Mech. **39**, 129–162 (2007).
[13] B. F. Farrel and P. J. Ioannou, "Optimal excitation of three-dimensional perturbations in viscous constant shear flow," Phys. Fluids A **6**, 1390–1400 (1993).
[14] T. Ellingsen and E. Palm, "Stability of linear flow," Phys. Fluids **18**, 487–488 (1975).
[15] M. T. Landahl, "Wave breakdown and turbulence," SIAM J. Appl. Math. **28**, 735–756 (1975).
[16] M. T. Landahl, "A note on an algebraic instability of inviscid parallel shear flows," J. Fluid Mech. **98**, 243–251 (1980).
[17] S. C. Reddy , P. J. Schmid, J. S. Baggett, and D. S. Henningson, "On stability of streamwise streaks and transition thresholds in plane channel flows," J. Fluid Mech. **365**, 269–303 (1998).
[18] F. Waleffe, "On a self-sustaining process in shear flows," Phys. Fluids **9**(4), 883–900 (1997).
[19] I. A. Frigaard, S. D. Howison, and I. J. Sobey, "On the stability of Poiseuille flow of a Bingham fluid," J. Fluid Mech. **263**, 133–150 (1994).
[20] C. Nouar and I. A. Frigaard, "Nonlinear stability of Poiseuille flow of Bingham fluids: Theoretical results and comparison with phenomenological criteria," J. Non-Newtonian Fluid Mech. **100**, 127–149 (2001).
[21] I. A. Frigaard and C. Nouar, "On three-dimensional linear stability of Poiseuille flow of Bingham fluids," Phys. Fluids **15**, 2843–2851 (2003).

[22] C. Nouar, N. Kabouya, J. Dusek, and M. Mamou, "Modal and non-modal linear stability of the plane Bingham-Poiseuille flow," J. Fluid Mech. **577**, 211–239 (2007).
[23] M. P. Escudier and F. Presti, "Pipe flow of a thixotropic liquid," J. Non-Newtonian Fluid Mech. **62**, 291–306 (1996).
[24] M. P. Escudier, R. J. Poole, F. Presti, C. Dales, C. Nouar, C. Desaubry, L. Grahamc, and L. Pullum, "Observations of asymmetrical flow behaviour in transitional pipe flow of yield-stress and other shear-thinning liquids," J. Non-Newtonian Fluid Mech. **127**, 143–155 (2005).
[25] J. Peixinho, C. Nouar, C. Desaubry, and B. Théron, "Laminar transitional and turbulent flow of yield stress fluid in a pipe," J. Non-Newtonian Fluid Mech. **128**, 172–184 (2005).
[26] A. Esmael and C. Nouar, "Transitional flow of a yield-stress fluid in a pipe: Evidence of a robust coherent structure," Phys. Rev. E **77**, 057302 (2008).
[27] A. Esmael, "Transition vers la turbulence pour un fluide á seuil en écoulement dans une conduite cylindrique," Ph.D. thesis, LEMTA UMR 7563 CNRS, INPL & UHP, Université Henri Poincaré, Nancy, 2008.
[28] B. Güzel, T. Burghelea, I. A. Frigaard, and D. M. Martinez, "Observation of laminar-turbulent transition of a yield stress fluid in Hagen-Poiseuille flow," J. Fluid Mech. **627**, 97–128 (2009).
[29] L. N. Trefethen and M. Embree, *Spectra and Pseudospectra: The Behavior of Nonnormal Matrices and Operators* (Princeton University Press, New Jersey, 2005).
[30] C. Canuto, M. Y. Hussaini, A. Quarteroni, and T. A. Zang, *Spectral Method in Fluid Dynamics* (Springer-Verlag New York, Inc., 1993).
[31] R. Liu and Q. S. Liu, "Nonmodal stability in Hagen-Poiseuille flow of a shear thinning fluid," Phys. Rev. E **85**, 066318 (2012).
[32] P. J. Schmid and D. S. Henningson, *Stability and Transition in Shear Flows* (Springer-Verlag New York, Inc., 2001).
[33] J. Pedlosky, *Geophysical Fluid Dynamics*, 2nd ed. (Springer-Verlag New York, Inc., 1987).